

Boosting Adversarial Transferability through Enhanced Momentum

Xiaosen Wang^{1*} Jiadong Lin^{1*} Han Hu² Jingdong Wang² Kun He^{1†}

¹School of Computer Science and Technology, Huazhong University of Science and Technology

²Microsoft Research Asia

{xiaosen, jdlin}@hust.edu.cn, {hanhu, jingdw}@microsoft.com, brooklet60@hust.edu.cn

Abstract

Deep learning models are known to be vulnerable to adversarial examples crafted by adding human-imperceptible perturbations on benign images. Many existing adversarial attack methods have achieved great white-box attack performance, but exhibit low transferability when attacking other models. Various momentum iterative gradient-based methods are shown to be effective to improve the adversarial transferability. In what follows, we propose an enhanced momentum iterative gradient-based method to further enhance the adversarial transferability. Specifically, instead of only accumulating the gradient during the iterative process, we additionally accumulate the average gradient of the data points sampled in the gradient direction of the previous iteration so as to stabilize the update direction and escape from poor local maxima. Extensive experiments on the standard ImageNet dataset demonstrate that our method could improve the adversarial transferability of momentum-based methods by a large margin of 11.1% on average. Moreover, by incorporating with various input transformation methods, the adversarial transferability could be further improved significantly. We also attack several extra advanced defense models under the ensemble-model setting, and the enhancements are remarkable with at least 7.8% on average.

1. Introduction

With the impressive performance of deep neural networks (DNNs) [11, 10, 8, 18, 4], the vulnerability to adversarial examples [29, 9], which are indistinguishable from legitimate ones by adding tiny perturbations but lead to erroneous predictions, has raised serious concerns in security-sensitive applications, *e.g.* self-driving automobile [7], face verification [25] *etc.* This issue of DNNs has triggered two research directions, with one trying to improve the attack

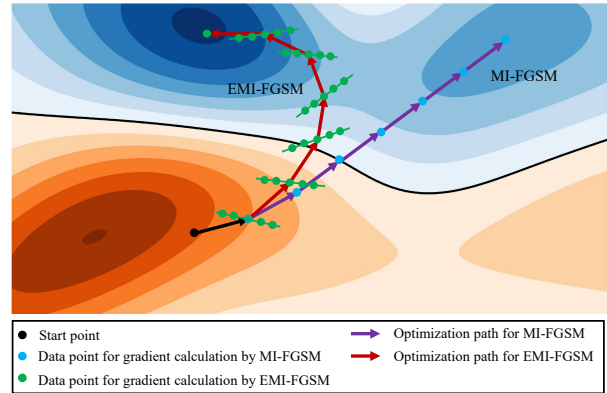


Figure 1: Illustration of the optimization path of MI-FGSM [5] and the proposed EMI-FGSM. At each iteration, MI-FGSM accumulates the gradient of data point along the path, while EMI-FGSM accumulates the accumulated gradient of sampled data points in the gradient direction of previous iteration. With such accumulation, EMI-FGSM can find better local maxima and exhibits higher transferability.

ability of adversarial examples [9, 12, 2, 1, 13] and the other line studying to improve the robustness of neural networks against the adversaries [19, 36, 14, 33, 3]. The two directions, namely *adversarial attack* and *adversarial defense*, usually act like spear and shield that the progress on one side can inspire the improvements of the other side.

For adversarial attack, numerous methods have been proposed in recent years, such as the one-step gradient-based attacks [9, 30], iterative gradient-based attacks [12, 19], and optimization-based attacks [29, 2]. Existing adversarial attacks often fall into the category of white-box setting, where the adversary is capable to access all information about the target model. For the counterpart category of black-box attacks, adversarial transferability, *i.e.* the ability of adversarial examples generated on one model to mislead other models, is an important metric. Such property makes it possible to attack deep neural models without knowing any in-

*The first two authors contribute equally.

†Corresponding author.

ner working mechanism in practice. Though white-box attacks achieve good attack performance, they often exhibit low transferability.

Recently, various methods have been proposed to improve the transferability of white-box attacks, *e.g.* incorporating momentum into iterative gradient-based attacks [5, 15], ensemble-model attack [16], input transformations [34, 6, 15, 31] *etc.* Note that both the ensemble-model attack and input transformations are based on existing gradient-based attacks. However, NI-FGSM, which exhibits the best transferability among existing momentum based attacks [15], can only achieve the average attack success rate of less than 52% under black-box setting, as shown in Table 1, indicating that the improvement of ensemble-model attack and transformation-based attack is rather limited.

In this work, inspired by the current momentum based attacks, we propose an enhanced momentum iterative fast gradient sign method, termed EMI-FGSM, to further promote the adversarial transferability. As shown in Figure 1, different from the existing momentum based methods (*e.g.* MI-FGSM) that just accumulate the gradients of data points along the optimization path, our enhanced momentum based method additionally accumulates the gradients of data points sampled in the gradient direction of previous iteration. Such accumulation might help find more stable direction of the gradient, leading to better local maxima. Empirical evaluations show that our method achieves higher attack success rates under white-box setting and exhibit significantly higher transferability under black-box setting.

Moreover, the proposed EMI-FGSM approach can work complementary to ensemble-model attacks and various input transformations. When integrated with these advanced methods, the enhanced momentum equipped methods can achieve significantly higher transferability on the standard ImageNet dataset than the state-of-the-art baselines. When attacking seven advanced defense models that exhibit good defense effectiveness against transferability on ImageNet, our method combined with input transformations under ensemble-model setting achieves an average attack success rate of 86.6%, improving the transferability of existing advanced methods by a clear margin of 7.8%.

2. Related Work

Given a classifier f and an input image x , where $f(x)$ outputs the prediction label of x . Let $J_f(x, y)$ denote the loss function of classifier f and $\mathcal{B}_\epsilon(x) = \{x' : \|x - x'\|_p \leq \epsilon\}$ denote the L_p -norm ball centered at x with radius ϵ and we focus on L_∞ -norm as in previous works.

2.1. Adversarial Attacks

Adversarial attacks can be formulated as finding an example $x^{adv} \in \mathcal{B}_\epsilon(x)$ that satisfies $f(x) \neq f(x^{adv})$. According to the threat model, existing adversarial attacks can

be roughly categorized into two settings: a) *white-box attack* allows full access to the threat model, *e.g.* model outputs, (hyper-)parameters, gradients and architectures, *etc.* b) *black-box attack* only allows access to the model outputs. Recent works also find that adversarial examples have good transferability [21, 16] across different models, *i.e.* the adversarial examples generated on one model can still fool other models, which falls into the black-box attacks.

Existing white-box adversarial attacks [29, 9, 12, 2, 19] usually optimize the perturbation based on the gradient and exhibit good attack performance but low transferability. To boost the transferability, several gradient-based adversarial attacks have been proposed. Dong *et al.* [5] propose to integrate momentum into iterative gradient-based attack. Lin *et al.* [15] propose to adopt Nestorve’s accelerated gradient to further enhance the transferability. Liu *et al.* [16] have shown that ensemble-model attack, which attacks multiple models simultaneously can improve the transferability.

Besides, recent works find that input transformations can further enhance the transferability of adversarial attacks. Diverse Input Method (DIM) [34] creates diverse input patterns by applying random resizing and padding to the input at each iteration before feeding the image into the model for gradient calculation. Translation-Invariant Method (TIM) [6] optimizes the perturbation over an ensemble of the translated images. To improve the efficiency, TIM convolves the gradient at the untranslated image with a pre-defined kernel, which needs one gradient calculation at each iteration. Scale-Invariant Method (SIM) [15] optimizes the adversarial perturbation over m scale copies of the input to achieve higher transferability.

Both the ensemble-model attack and input transformation based attacks can be combined with gradient-based methods to further improve the transferability. Our method is a new variation of the gradient-based attack that exhibits higher transferability and can be integrated with the ensemble-model attack and input transformation based methods to achieve higher transferability.

2.2. Adversarial Defenses

As the counterpart of adversarial attacks, numerous works have been proposed to strengthen the robustness of deep learning models. Adversarial training [9], one of the most promising defense methods [1, 13], which adopts adversarial examples for the training, has been extensively investigated by researchers [19, 30, 36, 26, 32]. Among different adversarial training variations, ensemble adversarial training [30], which adopts the adversarial examples generated on ensemble models, has been demonstrated to be robust against transfer-based adversarial attacks. Besides, several denoising or input preprocessing methods have also been proposed to mitigate adversarial effects. Liao *et al.* [14] propose a high-level representation guided denoiser

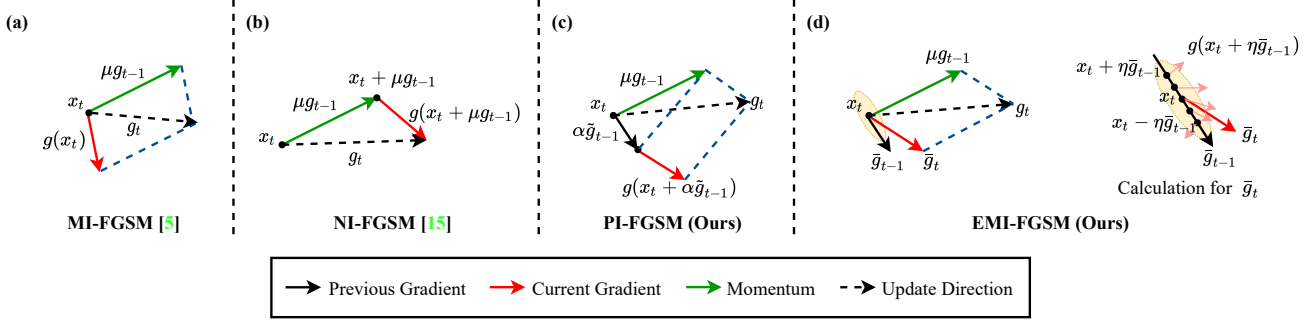


Figure 2: Illustration of the gradient update at the t -th iteration for various momentum based attack, where $g(x)$ denotes the gradient of x . (a) MI-FGSM [5] accumulates the gradient of x_t for update. (b) NI-FGSM [15] accumulates the gradient of $x_t + \mu g_{t-1}$ for update. (c) PI-FGSM accumulates the gradient of $x_t + \alpha \tilde{g}_{t-1}$ for update, where \tilde{g}_{t-1} is the gradient of the previous iteration. (d) EMI-FGSM accumulates the average gradient of the sampled data points in the direction of \bar{g}_{t-1} for update, where \bar{g}_{t-1} is the average gradient of the previous iteration.

(HGD) for purifying the adversarial examples. Xie *et al.* [33] apply random resizing and padding (R&P) to the input and feed the transformed image to the model to mitigate the adversarial effects. Feature distillation (FD) [17] is a JPEG-based defensive compression framework that can effectively rectify the adversarial examples without affecting the classification accuracy on benign images. Xu *et al.* [35] propose to use bit depth reduction (Bit-Red) of each pixel for feature squeezing to detect adversarial examples. Moreover, some works focus on certified robustness. Cohen *et al.* [3] propose to use randomized smoothing (RS) to train state-of-the-art certifiably ImageNet classifiers. Salman *et al.* [24] employ adversarial training to substantially improve the certified robustness of randomized smoothing (ARS).

3. Methodology

In this section, we first give an overview on the family of gradient-based adversarial attacks, to which our method belongs. Then we provide detailed descriptions of the proposed Pre-gradient guided momentum Iterative FGSM (PI-FGSM) and Enhanced Momentum I-FGSM (EMI-FGSM).

3.1. Gradient-based Adversarial Attacks

Gradient-based adversarial attacks are typical methods for adversarial attacks.

Fast Gradient Sign Method (FGSM) [9] generates adversarial examples by a one-step update:

$$x^{adv} = x + \epsilon \cdot \text{sign}(\nabla_x J_f(x, y)),$$

where $\text{sign}(\cdot)$ is the sign function and $\nabla_x J_f$ denotes the gradient of the loss function w.r.t. x .

Iterative Fast Gradient Sign Method (I-FGSM) [12] extends FGSM by iteratively applying the gradient updates:

$$x_{t+1}^{adv} = x_t^{adv} + \alpha \cdot \text{sign}(\nabla_{x_t^{adv}} J_f(x_t^{adv}, y)),$$

where $x_1^{adv} = x$, $\alpha = \epsilon/T$ is a small step size, and T is the number of iterations.

Momentum Iterative Fast Gradient Sign Method (MI-FGSM) [5] proposes to integrate the momentum [22] into the iterative attack to achieve higher transferability:

$$g_t = \mu \cdot g_{t-1} + \frac{\nabla_{x_t^{adv}} J_f(x_t^{adv}, y)}{\|\nabla_{x_t^{adv}} J_f(x_t^{adv}, y)\|_1},$$

$$x_{t+1}^{adv} = x_t^{adv} + \alpha \cdot \text{sign}(g_t),$$

where g_{t-1} is the accumulated gradient till the $(t-1)$ -th iteration with a decay factor μ and $g_0 = 0$.

Nesterov Iterative Fast Gradient Sign Method (NI-FGSM) [15] integrates Nesterov's accelerated gradient (NAG) [20] into the iterative attack method to further improve the transferability of adversarial examples:

$$\tilde{x}_t^{adv} = x_t^{adv} + \alpha \cdot \mu \cdot g_{t-1},$$

$$g_t = \mu \cdot g_{t-1} + \frac{\nabla_{\tilde{x}_t^{adv}} J_f(\tilde{x}_t^{adv}, y)}{\|\nabla_{\tilde{x}_t^{adv}} J_f(\tilde{x}_t^{adv}, y)\|_1},$$

$$x_{t+1}^{adv} = x_t^{adv} + \alpha \cdot \text{sign}(g_t).$$

3.2. Pre-gradient Guided Momentum based Attack

As shown in Figure 2 (a), MI-FGSM [5] accumulates the gradient of each iteration to stabilize the update direction and escape from poor local maxima, and achieves higher transferability than I-FGSM [12]. As depicted in Figure 2 (b), NI-FGSM *looks ahead* by accumulating the gradient after adding momentum to the current data point so as to converge faster and achieve higher transferability [15].

The performance improvement of NI-FGSM over MI-FGSM is mainly due to the *looking ahead* property of the Nesterov's accelerated gradient. We observe that NI-FGSM adopts the accumulated momentum in MI-FGSM to *look*

ahead, which is designed to obtain more stable direction by considering the history gradient. This inspires us to study a new problem: *Although the direction of accumulated momentum helps craft more transferable adversaries, is it the optimal direction for looking ahead?*

To explore the direction of *looking ahead*, we propose a variation of NI-FGSM, called the Pre-gradient guided momentum Iterative FGSM (PI-FGSM), which *looks ahead* by the gradient of the previous iteration. Specifically, as shown in Figure 2 (c), PI-FGSM accumulates the gradient of data point obtained by adding the previous gradient to the current data point at each iteration. The update procedure can be summarized as:

$$\begin{aligned}\tilde{x}_t^{adv} &= x_t^{adv} + \alpha \cdot \tilde{g}_{t-1}, \quad \tilde{g}_t = \nabla_{\tilde{x}_t^{adv}} J_f(\tilde{x}_t^{adv}, y), \\ g_t &= \mu \cdot g_{t-1} + \frac{\tilde{g}_t}{\|\tilde{g}_t\|_1}, \quad x_{t+1}^{adv} = x_t^{adv} + \alpha \cdot \text{sign}(g_t),\end{aligned}$$

where \tilde{g}_{t-1} denotes the gradient of the previous iteration. Instead of considering all the history gradient as in NI-FGSM, PI-FGSM *looks ahead* guided by the local gradient information and achieves better attack performance, as demonstrated in Sec. 4.2.

3.3. Enhanced Momentum based Attack

We continue to investigate the family of momentum based attacks and observe that at each iteration, MI-FGSM [5], NI-FGSM [15] and our PI-FGSM accumulate the gradient of different data points, and they all exhibit higher transferability than I-FGSM [12] that only adopts the gradient of the current data point for update. This indicates that the accumulation of gradient is helpful for crafting highly transferable adversaries. Since the accumulation of gradient of these methods are on different data points, this inspires us another question: *At each iteration, could we further improve the attack transferability by accumulating the gradients of multiple data points around the current data point for the iterative gradient-based attacks?*

To address this question, we enhance the momentum by not only memorizing all the past gradients during the iterative process, but also accumulating the gradients of multiple sampled examples in the vicinity of the current data point. Considering the performance improvement of PI-FGSM, to help sample more useful data points for the gradient calculation, we sample multiple data points along the direction used in PI-FGSM, *i.e.* the gradient direction of the previous iteration. Specifically, as shown in Figure 2 (d), we calculate the gradient of the t -th iteration as follows:

$$\tilde{x}_t^{adv}[i] = x_t^{adv} + c_i \cdot \tilde{g}_{t-1} \quad (1)$$

$$\tilde{g}_t = \frac{1}{N} \sum_{i=1}^N \nabla_{\tilde{x}_t^{adv}[i]} J_f(\tilde{x}_t^{adv}[i], y), \quad (2)$$

Algorithm 1 EMI-FGSM.

Input: A classifier f and loss function J_f . A benign example x and its ground-truth label y .

Input: The maximum perturbation ϵ , number of iteration T and decay factor μ . The bound η for the sampling interval and sampling number N .

Output: An adversarial example $x^{adv} \in \mathcal{B}_\epsilon(x)$.

1: $\alpha = \epsilon/T$; $g_0 = 0$; $\bar{g}_0 = 0$; $x_1^{adv} = x$.

2: **for** $t = 1 \rightarrow T$ **do**:

3: Sample N coefficients $c_i \in [-\eta, \eta]$ for Eq. (1).

4: Calculate the average gradient \bar{g}_t of the N sampled data points in the neighborhood of x_t^{adv} by Eq. (2).

5: Update the enhanced momentum g_t by Eq. (3).

6: Update x_{t+1}^{adv} by Eq. (4).

7: **end for**

8: **return** $x^{adv} = x_{T+1}^{adv}$.

where N is the sampling number, \bar{g}_{t-1} is the gradient calculated at the previous iteration and c_i is the i -th coefficient sampled in interval $[-\eta, \eta]$. We denote such accumulated gradient as the enhanced momentum.

Note that the proposed enhanced momentum is generally applicable to any iterative gradient-based attacks, such as I-FGSM [12], PGD [19], and the ensemble-model attack [16]. Here we incorporate the enhanced momentum into I-FGSM, denoted as Enhanced Momentum I-FGSM (EMI-FGSM), to craft highly transferable adversarial examples. The update procedure can be summarized as:

$$g_t = \mu \cdot g_{t-1} + \frac{\bar{g}_t}{\|\bar{g}_t\|_1}, \quad (3)$$

$$x_{t+1}^{adv} = x_t^{adv} + \alpha \cdot \text{sign}(g_t), \quad (4)$$

where \bar{g}_t is the gradient calculated by Eq. (2). The algorithm of EMI-FGSM is summarized in Algorithm 1. For other possible sampling methods, we have also tried to sample the data points in the direction of NI-FGSM or do random sampling, but the sampling in the direction of PI-FGSM exhibits better results, as discussed in Sec. 4.6.

4. Experiments

In this section, we provide the experimental setup, report comparisons of gradient-based attacks on four normally trained models and comparisons when integrated with transformation-based attacks and ensemble-model attack, as well as results of attacking seven advanced defense models. In the end, we further provide ablation studies for the sampling method and hyper-parameters as well as discussions on other possible variant methods.

4.1. Experimental Setup

Dataset. Similar to [34, 15], we randomly choose 1,000 images from the ILSVRC 2012 validation set [23]. All these

Attack	Inc-v3*	Inc-v4	IncRes-v2	Res-101	Inc-v3 _{ens3}	Inc-v3 _{ens4}	IncRes-v2 _{ens}
FGSM	67.3	25.7	26.0	24.5	10.2	10.4	4.5
I-FGSM	100.0	20.3	18.5	16.1	4.6	5.2	2.5
MI-FGSM	100.0	44.5	42.0	36.3	13.4	13.7	6.5
NI-FGSM	100.0	51.9	50.4	41.0	13.4	13.2	5.7
PI-FGSM (Ours)	100.0	60.2	59.1	49.0	14.9	14.6	6.5
EMI-FGSM (Ours)	100.0	72.7	69.9	59.5	20.3	19.9	10.9

Table 1: **Attack success rates (%) of adversarial attacks against the seven baseline models under single-model setting.** The adversarial examples are crafted on Inc-v3. * indicates the white-box model being attacked.

Attack	Inc-v3*	Inc-v4*	IncRes-v2*	Res-101*	Inc-v3 _{ens3}	Inc-v3 _{ens4}	IncRes-v2 _{ens}
FGSM	64.8	49.3	43.9	68.8	15.8	15.1	8.9
I-FGSM	99.9	98.6	95.6	99.8	19.1	16.8	10.4
MI-FGSM	99.9	98.7	95.0	99.9	39.7	35.5	23.8
NI-FGSM	100.0	99.8	99.2	99.9	41.2	34.9	22.9
PI-FGSM (Ours)	100.0	99.2	98.5	99.9	52.5	45.3	29.6
EMI-FGSM (Ours)	100.0	99.8	99.8	100.0	69.0	62.0	43.0

Table 2: **Attack success rates (%) of adversarial attacks against the seven baseline models under ensemble-model setting.** The adversarial examples are crafted on ensemble models including Inc-v3, Inc-v4, IncRes-v2 and Res-101.

images are resized to $299 \times 299 \times 3$ beforehand.

Baselines. We compare our method with four gradient-based attack methods including FGSM [9], I-FGSM [12], MI-FGSM [5] and NI-FGSM [15]. We also integrate our method into the ensemble-model attack [16, 5] and input transformation based methods [34, 6, 15], to show the performance improvement of our method over these baselines.

Models. Four normally trained models, *i.e.* Inception-v3 (Inc-v3) [28], Inception-v4 (Inc-v4), Inception-Resnet-v2 (IncRes-v2) [27], Resnet-v2-101 (Res-101) [10], as well as three ensemble adversarially trained models, *i.e.* ens3-adv-Inception-v3 (Inc-v3_{ens3}), ens4-Inception-v3 (Inc-v3_{ens4}), ens-adv-Inception-ResNet-v2 (IncRes-v2_{ens}) [30], are considered. Without ambiguity, we simply call the three ensemble adversarially trained models as *adversarially trained models*. Moreover, to show the efficacy of our methods, we also incorporate seven advanced defense methods, including the top-3 submission in the NIPS 2017 defense competition, *i.e.* high-level representation guided denoiser (HGD, rank-1) [14], input transformation through random resizing and padding (R&P, rank-2) [33], NIPS-r3 (rank-3)¹, randomized smoothing (RS) [3] and adversarially randomized smoothing (ARS) [24] for certified defense, feature distillation (FD) [17] and bit depth reduction (Bit-Red) [35].

Attack Settings. We follow the settings in [5] with the maximum perturbation of $\epsilon = 16/255$, pixel values normalized into $[0, 1]$ and the number of iteration $T = 10$. For the momentum term, we set the decay factor $\mu = 1$ as in [5, 15]. For DIM, we set the transformation probability to 0.5 and the input x is first randomly resized to an $r \times r \times 3$ image with $r \in [299, 330]$, and then padded to size $330 \times 330 \times 3$

¹<https://github.com/anlthms/nips-2017/tree/master/mmd>

as in [34]. For TIM, we adopt Gaussian kernel with size 7×7 as in [6]. For SIM, the number of scale copy is set to $m = 5$ as in [15]. For EMI-FGSM, we set the number of examples N to 11, set the sampling interval bound $\eta = 7$, and adopt the linear sampling.

4.2. Comparison with Gradient-based Attacks

We first craft adversaries by various gradient-based attacks under single-model setting and ensemble-model setting respectively, and report the attack success rates, which are the misclassification rates of the corresponding models using adversarial examples as the inputs.

Single-model Setting. The results for adversarial examples crafted on Inc-v3 are depicted in Table 1 and the results on other three normally trained models are summarized in Appendix. We can see that except for FGSM, all the other attacks achieve 100% attack success rates under white-box setting. For black-box attacks, I-FGSM achieve the transferability even lower than FGSM. Compared with MI-FGSM and NI-FGSM, the transferability of the proposed PI-FGSM is much higher (8-9%) on normally trained models, and is considerably higher (0.8-1.5%) on adversarially trained models. With the enhanced momentum, EMI-FGSM exhibits much higher transferability on both normally trained models (10.5-12.5% higher than PI-FGSM) and adversarially trained models (4.4-5.4% higher than PI-FGSM), and outperforms the powerful baseline NI-FGSM with a clear margin of 11.1% on average.

Ensemble-model Setting. As in [5], we implement the attacks under ensemble-model setting by fusing the logit outputs of four normally trained models, *i.e.* Inc-v3, Inc-v3, IncRes-v2 and Res-101, with equal ensemble weights. As shown in Table 2, the proposed PI-FGSM exhibits bet-

Attack	Inc-v3*	Inc-v4	IncRes-v2	Res-101	Inc-v3 _{ens3}	Inc-v3 _{ens4}	IncRes-v2 _{ens}
DIM	99.0	64.6	60.9	52.1	18.3	17.7	9.5
EMI-DIM (Ours)	99.1	83.5	78.0	70.6	27.8	26.0	13.4
TIM	100.0	47.0	44.5	40.5	24.3	22.0	13.2
EMI-TIM (Ours)	100.0	79.4	76.3	67.2	44.3	40.8	26.2
SIM	100.0	70.3	68.0	62.4	32.4	30.8	17.2
EMI-SIM (Ours)	100.0	91.9	90.0	85.4	45.2	41.8	23.8
DTS	98.9	83.1	80.7	75.8	65.2	62.7	46.0
EMI-DTS (Ours)	99.6	94.1	92.6	89.4	78.9	75.3	60.4

Table 3: **Attack success rates (%) of adversarial attacks against the seven baseline models under single-model setting.** The adversarial examples are crafted on Inc-v3.

Attack	Inc-v3*	Inc-v4*	IncRes-v2*	Res-101*	Inc-v3 _{ens3}	Inc-v3 _{ens4}	IncRes-v2 _{ens}
DIM	99.4	97.4	94.7	99.8	56.3	50.7	36.4
EMI-DIM (Ours)	99.9	99.6	99.7	99.7	77.0	70.1	50.3
TIM	99.8	98.0	95.0	99.9	61.3	56.7	47.8
EMI-TIM (Ours)	100.0	100.0	99.7	100.0	89.0	83.9	78.2
SIM	99.9	99.3	98.5	100.0	78.5	74.4	60.4
EMI-SIM (Ours)	100.0	100.0	100.0	100.0	90.1	87.3	74.2
DTS	99.6	98.9	97.9	99.7	92.1	90.2	86.6
EMI-DTS (Ours)	100.0	99.9	100.0	100.0	97.4	96.1	94.1

Table 4: **Attack success rates (%) of adversarial attacks against the seven baseline models under ensemble-model setting.** The adversarial examples are crafted on ensemble models including Inc-v3, Inc-v4, IncRes-v2 and Res-101.

ter attack success rates than I-FGSM and MI-FGSM under white-box setting and achieves much higher transferability on three adversarially trained models. This validates our first concern that due to considering too much history gradient, the accumulated momentum adopted by NI-FGSM provide imprecise direction compared with PI-FGSM, which is not optimal for looking ahead. Moreover, EMI-FGSM achieve the best results under both white-box and black-box setting and outperforms the powerful baseline NI-FGSM by a large margin of more than 20%, which demonstrates the high effectiveness of the proposed enhanced momentum.

4.3. Integrated with Transformation-based Attacks

We further incorporate EMI-FSGM with various input transformations, *i.e.* DIM, TIM, SIM, and the combination of the three input transformations, denoted as DTS for abbreviation, under single-model setting and ensemble-model setting respectively. To ensure fairness, all the transformations are integrated into MI-FGSM as baselines [34, 6].

Single-model Setting. The results for adversaries generated on Inc-v3 are summarized in Tabel 3. We can observe that EMI can significantly boost the transferability on each of the transformation-based attack methods. In general, the EMI based attacks consistently outperform the baseline attacks by 3.9% \sim 32.4%. Even for white-box setting, EMI further promotes the attack success rates of the baseline attacks. For instance, EMI-DTS outperforms DTS by 0.7% against Inc-v3. The results for adversarial examples crafted on other three normally-trained models are consistent with that generated on Inc-v3, that are summarized in Appendix.

Ensemble-model Setting. As in Sec. 4.2, we also evaluate the attacks under ensemble-model setting and the results are summarized in Table 4. EMI based method remarkably improves the attack success rates across all experiments over the baseline attacks. In particular, the final combination of EMI-DTS has achieved the attack success rates of over 94.1% for black-box attacks against the three adversarially trained models. Such intriguing results convincingly demonstrate the success on the combination of EMI-FGSM, input transformations and ensemble-model attack for improving the attack transferability.

4.4. Attacking Advanced Defense Models

With the significant improvement on the attack baselines, we further evaluate EMI-FGSM on seven advanced defense models with various input transformations under ensemble-model setting to demonstrate its high efficacy. All the adversaries are generated on the ensemble models as in Sec. 4.3 and we test the advanced defenses with these adversaries.

The results of EMI-FGSM with three transformation-based attacks are illustrated in Figure 3a-3c. As can be observed, EMI-FGSM remarkably improves the transferability of the three transformation-based attacks on all these defense equipped models. On average, the performances are improved by 14.8%, 24.5% and 11.8% respectively. Moreover, we also integrate the combination of the three input transformations into EMI-FGSM as in [15] to further improve the transferability. As shown in Figure 3d, EMI-DTS achieves an average attack success rate of 86.6%, which boosts existing state-of-the-art methods by a clear margin

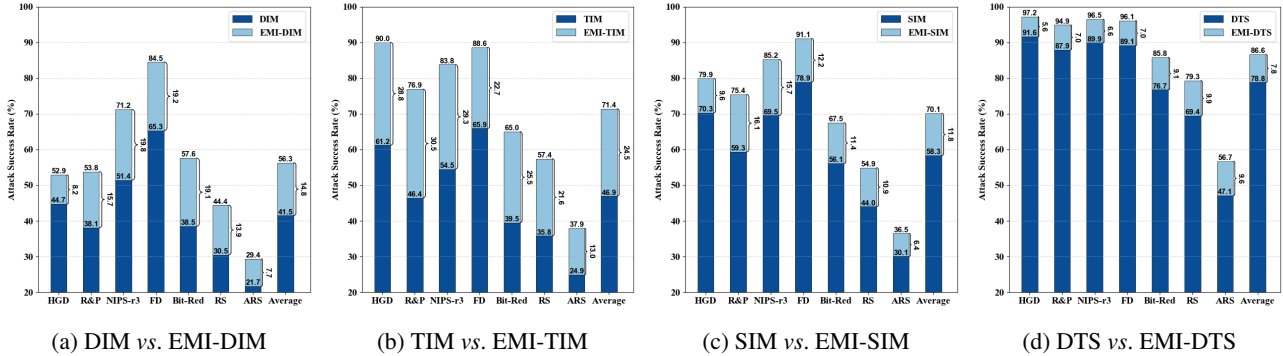


Figure 3: **Attack success rates (%) of adversarial attacks against seven advanced defense methods.** The adversarial examples are crafted on the ensemble models including Inc-v3, Inc-v4, IncRes-v2, and Res-101. (Zoom in for details.)

Attack	Sampling Method	Inc-v3*	Inc-v4	IncRes-v2	Res-101	Inc-v3 _{ens3}	Inc-v3 _{ens4}	IncRes-v2 _{ens}
EMI-FGSM	Linear	100.0	74.4	71.9	60.5	21.2	19.5	9.9
	Uniform	100.0	74.7	71.5	61.2	18.9	18.8	8.8
	Gaussian	100.0	73.0	70.4	60.0	20.2	19.0	9.9
EMI-DTS	Linear	99.6	94.5	92.8	90.2	78.8	76.0	60.3
	Uniform	99.5	92.9	91.9	87.9	77.1	71.5	57.0
	Gaussian	99.5	94.8	92.6	89.7	78.5	74.3	58.7

Table 5: **Attack success rates (%) of EMI-FGSM and EMI-DTS against the seven baseline models with various sampling methods.** The adversarial examples are crafted on Inc-v3.

of 7.8%. Considering that the adversaries are crafted on the ensemble models without any defense mechanisms but with such high attack performance, the results identify the inefficiency of existing defenses and indicate that they are far from being deployed in real-world applications.

4.5. Ablation Study

To gain more insights on the performance improvement by our enhanced momentum based methods, we conduct ablation studies to explore the impact of the sampling method and the hyper-parameters for the sampling interval η and sampling number N , respectively. To simplify the analysis, we only consider the transferability of adversarial examples crafted on Inc-v3 model by vanilla EMI-FGSM and EMI-DTS. The default setting adopts linear sampling, and we set $\eta = 7$ and $N = 11$.

On sampling distribution. We first report the results of EMI-FGSM and EMI-DTS with three types of sampling methods, *i.e.*, linear sampling, uniform sampling and Gaussian sampling. Linear sampling samples N linearly spaced data points in the interval. Uniform sampling and Gaussian sampling sample N data points in the interval by uniform distribution and Gaussian distribution, respectively. As shown in Table 5, the three sampling methods achieve similar attack performance, showing much higher transferability than the attack baselines. In general, linear sampling exhibits slightly higher results, thus we adopt linear sam-

pling in experiments.

On sampling interval. The sampling interval η also plays a key role in improving the attack performance. We try different values of η from 1 to 10 and the results are summarized in Figure 4. For all the values of η , the white-box attack success rate is 100%. The transferability increases when $\eta \leq 3$ for both EMI-FGSM and EMI-DTS. For $4 \leq \eta \leq 7$, the attacks exhibit similar transferability and the performance decays slightly when $\eta > 7$. Thus we adopt $\eta = 7$ in experiments.

On sampling number. We continue to explore the impact of the sampling number N , as illustrated in Figure 5. The white-box attack success rate for various values of N is 100%. When $N = 1$, EMI-FGSM degrades to MI-FGSM and exhibits the lowest transferability. When we increase the value of N , the transferability increases rapidly before $N = 11$ for EMI-FGSM and $N = 7$ for EMI-DTS. When $N > 11$, increasing N can still bring small performance improvement for EMI-FGSM. However, the bigger the value of N , the higher the computational cost. To balance the performance gain and the cost, we set $N = 11$ in experiments.

4.6. Discussion on Possible Variations

Except for EMI-FGSM, there are also other ways to enhance the momentum. Here we provide two possible implementations of the enhanced momentum, denoted as ENI-FGSM and ERI-FGSM. Specifically, ENI-FGSM samples

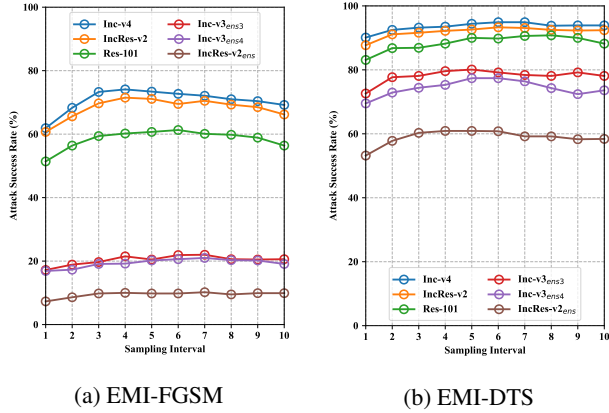


Figure 4: Attack success rates (%) on the other six models with adversarial examples generated by EMI-FGSM and EMI-DTS on Inc-v3 for various **sampling interval**.

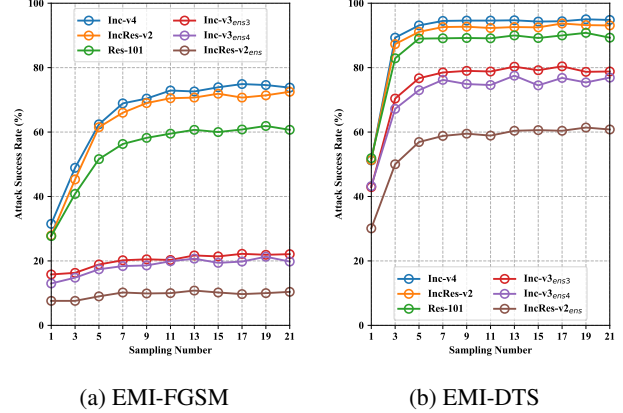


Figure 5: Attack success rates (%) on the other six models with adversarial examples generated by EMI-FGSM and EMI-DTS on Inc-v3 for various **sampling number**.

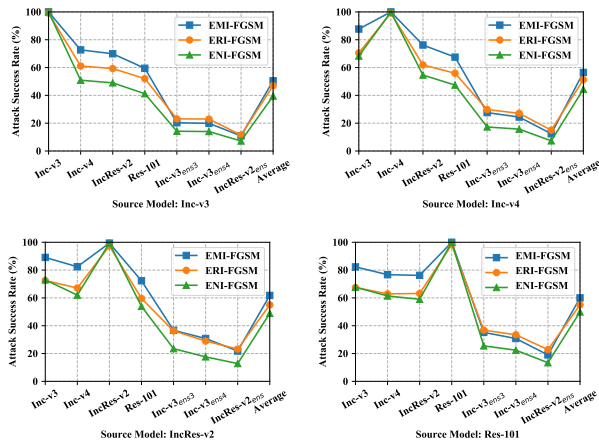


Figure 6: Attack success rates (%) of EMI-FGSM, ERI-FGSM and ENI-FGSM against the seven models under single-model setting.

the data points in the direction of momentum by substituting Eq. 1 in EMI-FGSM with:

$$\bar{x}_t^{adv}[i] = x_t^{adv} + c_i \cdot g_{t-1} \quad (5)$$

where g_{t-1} is the accumulated momentum of the previous iteration. ERI-FGSM adopts the accumulated gradient of randomly sampled data points by substituting Eq. 1 in EMI-FGSM with:

$$\bar{x}_t^{adv}[i] = x_t^{adv} + \alpha \cdot U(-1^d, 1^d) \quad (6)$$

where $U(a, b)$ denotes the uniform distribution in $[a, b]$.

EMI-FGSM vs. ENI-FGSM. The proposed EMI-FGSM accumulates the gradient of the data points in the direction of $(t-1)$ -th gradient at the t -th iteration and exhibits remarkable performance improvement. However, from the perspective of NI-FGSM, *can we accumulate the gradient*

of the data points in the direction of momentum at the t -th iteration? To address this concern, we extend NI-FGSM to ENI-FGSM and test the attack performance. As shown in Figure 6, we see that ENI-FGSM is considerably lower than EMI-FGSM. It further supports our hypothesis that the direction of the accumulated momentum cannot provide a precise description of the neighborhood and find proper point for the gradient calculation, as it contains too much accumulated information from the previous iterations.

EMI-FGSM vs. ERI-FGSM. The comparison between ENI-FGSM and EMI-FGSM shows that the direction plays a big impact on the performance of the enhanced momentum. Both ENI-FGSM and EMI-FGSM sample the data points in a fixed direction. *What if we accumulate the gradient of the data points in the neighborhood of x_t^{adv} at the t -th iteration?* To address this concern, we test the performance of ERI-FGSM on various models. As shown in Figure 6, ERI-FGSM exhibits considerably lower transferability than EMI-FGSM on normally trained models but achieves slightly better performance on adversarially trained models. A possible reason might be that the data points with noise for the gradient calculation are more similar to the adversaries for the adversarial training.

5. Conclusion

Inspired by existing momentum based attacks, we propose an enhanced momentum method that not only accumulates the gradient of each iteration, but also accumulates the gradients of the sampled data points in the gradient direction of previous iteration. We then incorporate our enhanced momentum method into the iterative gradient-based methods to strengthen the adversarial attacks, which can significantly improve the attack success rates under white-box as well as black-box settings, as evaluated on the standard ImageNet dataset. Our strongest enhanced momentum based

attack, the EMI-DTS that is integrated with existing input transformations under the ensemble-model setting, could achieve an average black-box attack success rates of over 94%, showing very high adversarial transferability. Our work also indicates that existing defenses are far from being deployed in real-world applications and stronger robust deep learning models are needed.

References

- [1] Anish Athalye, Nicholas Carlini, and David Wagner. Obfuscated gradients give a false sense of security: Circumventing defenses to adversarial examples. *International Conference on Machine Learning (ICML)*, 2018. 1, 2
- [2] Nicholas Carlini and David Wagner. Towards evaluating the robustness of neural networks. In *2017 IEEE Symposium on Security and Privacy (SP)*, pages 39–57, 2017. 1, 2
- [3] Jeremy M Cohen, Elan Rosenfeld, and J Zico Kolter. Certified adversarial robustness via randomized smoothing. *International Conference on Machine Learning (ICML)*, 2019. 1, 3, 5
- [4] Jacob Devlin, Ming-Wei Chang, Kenton Lee, and Kristina Toutanova. Bert: Pre-training of deep bidirectional transformers for language understanding. *Proceedings of the Conference of the North American Chapter of the Association for Computational Linguistics: Human Language Technologies (NAACL-HLT)*, 2019. 1
- [5] Yinpeng Dong, Fangzhou Liao, Tianyu Pang, Hang Su, Jun Zhu, Xiaolin Hu, and Jianguo Li. Boosting adversarial attacks with momentum. In *Proceedings of the IEEE Conference on Computer Vision and Pattern Recognition (CVPR)*, pages 9185–9193, 2018. 1, 2, 3, 4, 5
- [6] Yinpeng Dong, Tianyu Pang, Hang Su, and Jun Zhu. Evading defenses to transferable adversarial examples by translation-invariant attacks. In *Proceedings of the IEEE Conference on Computer Vision and Pattern Recognition (CVPR)*, pages 4312–4321, 2019. 2, 5, 6
- [7] Kevin Eykholt, Ivan Evtimov, Earlene Fernandes, Bo Li, Amir Rahmati, Chaowei Xiao, Atul Prakash, Tadayoshi Kohno, and Dawn Song. Robust physical-world attacks on deep learning visual classification. In *Proceedings of the IEEE Conference on Computer Vision and Pattern Recognition (CVPR)*, pages 1625–1634, 2018. 1
- [8] Ross Girshick. Fast r-cnn. In *Proceedings of the IEEE International Conference on Computer Vision (ICCV)*, pages 1440–1448, 2015. 1
- [9] Ian J Goodfellow, Jonathon Shlens, and Christian Szegedy. Explaining and harnessing adversarial examples. *International Conference on Learning Representations (ICLR)*, 2015. 1, 2, 3, 5
- [10] Kaiming He, Xiangyu Zhang, Shaoqing Ren, and Jian Sun. Deep residual learning for image recognition. In *Proceedings of the IEEE conference on computer vision and pattern recognition (CVPR)*, pages 770–778, 2016. 1, 5
- [11] Alex Krizhevsky, Ilya Sutskever, and Geoffrey E Hinton. Imagenet classification with deep convolutional neural networks. In *Advances in Neural Information Processing Systems (NIPS)*, pages 1097–1105, 2012. 1
- [12] Alexey Kurakin, Ian Goodfellow, and Samy Bengio. Adversarial examples in the physical world. *International Conference on Learning Representations (ICLR), Workshop Track Proceedings*, 2017. 1, 2, 3, 4, 5
- [13] Yandong Li, Lijun Li, Liqiang Wang, Tong Zhang, and Boqing Gong. Nattack: Learning the distributions of adversarial examples for an improved black-box attack on deep neural networks. *International Conference on Machine Learning (ICML)*, 2019. 1, 2
- [14] Fangzhou Liao, Ming Liang, Yinpeng Dong, Tianyu Pang, Xiaolin Hu, and Jun Zhu. Defense against adversarial attacks using high-level representation guided denoiser. In *Proceedings of the IEEE Conference on Computer Vision and Pattern Recognition (CVPR)*, pages 1778–1787, 2018. 1, 2, 5
- [15] Jiadong Lin, Chuanbiao Song, Kun He, Liwei Wang, and John E Hopcroft. Nesterov accelerated gradient and scale invariance for adversarial attacks. In *International Conference on Learning Representations (ICLR)*, 2020. 2, 3, 4, 5, 6
- [16] Yanpei Liu, Xinyun Chen, Chang Liu, and Dawn Song. Delving into transferable adversarial examples and black-box attacks. *International Conference on Learning Representations (ICLR)*, 2017. 2, 4, 5
- [17] Zihao Liu, Qi Liu, Tao Liu, Nuo Xu, Xue Lin, Yanzhi Wang, and Wujie Wen. Feature distillation: Dnn-oriented jpeg compression against adversarial examples. In *Proceedings of the IEEE Conference on Computer Vision and Pattern Recognition (CVPR)*, pages 860–868, 2019. 3, 5
- [18] Jonathan Long, Evan Shelhamer, and Trevor Darrell. Fully convolutional networks for semantic segmentation. In *Proceedings of the IEEE conference on computer vision and pattern recognition (CVPR)*, pages 3431–3440, 2015. 1
- [19] Aleksander Madry, Aleksandar Makelov, Ludwig Schmidt, Dimitris Tsipras, and Adrian Vladu. Towards deep learning models resistant to adversarial attacks. *International Conference on Learning Representations (ICLR)*, 2018. 1, 2, 4
- [20] Yurii Nesterov. A method for unconstrained convex minimization problem with the rate of convergence $o(1/k^2)$. *Doklady AN USSR*, 269:543–547, 1983. 3
- [21] Nicolas Papernot, Patrick McDaniel, Ian Goodfellow, Somesh Jha, Z Berkay Celik, and Ananthram Swami. Practical black-box attacks against machine learning. In *Proceedings of the 2017 ACM on Asia Conference on Computer and Communications Security*, pages 506–519, 2017. 2
- [22] Boris T Polyak. Some methods of speeding up the convergence of iteration methods. *Ussr computational mathematics and mathematical physics*, 4(5):1–17, 1964. 3
- [23] Olga Russakovsky, Jia Deng, Hao Su, Jonathan Krause, Sanjeev Satheesh, Sean Ma, Zhiheng Huang, Andrej Karpathy, Aditya Khosla, Michael Bernstein, et al. Imagenet large scale visual recognition challenge. *International Journal of Computer Vision (IJCV)*, 115(3):211–252, 2015. 4
- [24] Hadi Salman, Jerry Li, Ilya Razenshteyn, Pengchuan Zhang, Huan Zhang, Sebastien Bubeck, and Greg Yang. Provably robust deep learning via adversarially trained smoothed classifiers. In *Advances in Neural Information Processing Systems (NeurIPS)*, pages 11292–11303, 2019. 3, 5
- [25] Mahmood Sharif, Sruti Bhagavatula, Lujo Bauer, and Michael K Reiter. Accessorize to a crime: Real and stealthy

- attacks on state-of-the-art face recognition. In *Proceedings of the 2016 ACM Sigsac Conference on Computer and Communications Security*, pages 1528–1540, 2016. 1
- [26] Chuanbiao Song, Kun He, Liwei Wang, and John E Hopcroft. Improving the generalization of adversarial training with domain adaptation. *International Conference on Learning Representations (ICLR)*, 2019. 2
- [27] Christian Szegedy, Sergey Ioffe, Vincent Vanhoucke, and Alex Alemi. Inception-v4, inception-resnet and the impact of residual connections on learning. *AAAI Conference on Artificial Intelligence (AAAI)*, 2017. 5
- [28] Christian Szegedy, Vincent Vanhoucke, Sergey Ioffe, Jon Shlens, and Zbigniew Wojna. Rethinking the inception architecture for computer vision. In *Proceedings of the IEEE conference on computer vision and pattern recognition (CVPR)*, pages 2818–2826, 2016. 5
- [29] Christian Szegedy, Wojciech Zaremba, Ilya Sutskever, Joan Bruna, Dumitru Erhan, Ian Goodfellow, and Rob Fergus. Intriguing properties of neural networks. *International Conference on Learning Representations (ICLR)*, 2014. 1, 2
- [30] Florian Tramèr, Alexey Kurakin, Nicolas Papernot, Ian Goodfellow, Dan Boneh, and Patrick McDaniel. Ensemble adversarial training: Attacks and defenses. *International Conference on Learning Representations (ICLR)*, 2018. 1, 2, 5
- [31] Xiaosen Wang, Xuanran He, Jingdong Wang, and Kun He. Admix: Enhancing the transferability of adversarial attacks. *arXiv preprint arXiv:2102.00436*, 2021. 2
- [32] Yisen Wang, Difan Zou, Jinfeng Yi, James Bailey, Xingjun Ma, and Quanquan Gu. Improving adversarial robustness requires revisiting misclassified examples. In *International Conference on Learning Representations (ICLR)*, 2020. 2
- [33] Cihang Xie, Jianyu Wang, Zhishuai Zhang, Zhou Ren, and Alan Yuille. Mitigating adversarial effects through randomization. *International Conference on Learning Representations (ICLR)*, 2018. 1, 3, 5
- [34] Cihang Xie, Zhishuai Zhang, Yuyin Zhou, Song Bai, Jianyu Wang, Zhou Ren, and Alan L Yuille. Improving transferability of adversarial examples with input diversity. In *Proceedings of the IEEE Conference on Computer Vision and Pattern Recognition (CVPR)*, pages 2730–2739, 2019. 2, 4, 5, 6
- [35] Weilin Xu, David Evans, and Yanjun Qi. Feature squeezing: Detecting adversarial examples in deep neural networks. *Network and Distributed System Security Symposium (NDSS)*, 2018. 3, 5
- [36] Hongyang Zhang, Yaodong Yu, Jiantao Jiao, Eric P Xing, Laurent El Ghaoui, and Michael I Jordan. Theoretically principled trade-off between robustness and accuracy. *International Conference on Machine Learning (ICML)*, 2019. 1, 2

Appendix

In the supplementary material, we report the comparison results on various gradient-based attack methods and our EMI-FGSM method integrated with various transformation-based methods when attacking the other three normally trained models, *i.e.* Inc-v4, IncRes-v2, and Res-101 respectively.

We first report the attack success rates of various gradient-based attack methods on the other three normally-trained models. The results are summarized in Table 6. Compared with other advanced attacks, EMI-FGSM also exhibits better white-box attack success rates and higher transferability, which are consistent to the results on the Inc-v3 model in the main text.

The results for the EMI-FGSM integrated with various transformation-based methods under single-model setting, where the adversarial examples are crafted on the other three normally-trained models, are depicted in Table 7. It can be observed that EMI significantly promotes the attack success rates of the baseline attacks with a clear margin, which are consistent to the results on the Inc-v3 model in the main text and further verifies the high effectiveness of the proposed enhanced momentum.

Attack	Inc-v3	Inc-v4*	IncRes-v2	Res-101	Inc-v3 _{ens3}	Inc-v3 _{ens4}	IncRes-v2 _{ens}
FGSM	27.4	52.0	22.5	22.9	15.7	9.4	5.4
I-FGSM	32.8	100.0	20.0	19.9	5.3	6.8	3.1
MI-FGSM	56.2	99.9	46.0	40.7	15.7	15.1	8.3
NI-FGSM	63.0	99.9	52.4	45.6	16.5	14.3	7.5
PI-FGSM (Ours)	72.4	99.9	59.7	52.5	18.0	15.7	7.3
EMI-FGSM (Ours)	87.7	100.0	76.2	67.5	27.6	24.4	12.4

(a) Attack success rates (%) for the adversarial examples crafted on **Inc-v4**.

Attack	Inc-v3	Inc-v4	IncRes-v2*	Res-101	Inc-v3 _{ens3}	Inc-v3 _{ens4}	IncRes-v2 _{ens}
FGSM	27.2	20.2	41.9	23.6	9.5	9.1	5.7
I-FGSM	33.4	25.2	98.2	20.2	6.8	6.4	4.3
MI-FGSM	57.3	50.4	98.2	44.7	21.2	16.0	11.5
NI-FGSM	63.4	55.9	99.0	45.3	20.2	15.8	10.0
PI-FGSM (Ours)	71.6	63.4	98.3	53.4	24.3	18.7	12.5
EMI-FGSM (Ours)	89.1	82.4	99.4	72.3	36.7	30.8	21.8

(b) Attack success rates (%) for the adversarial examples crafted on **IncRes-v2**.

Attack	Inc-v3	Inc-v4	IncRes-v2	Res-101*	Inc-v3 _{ens3}	Inc-v3 _{ens4}	IncRes-v2 _{ens}
FGSM	36.4	31.2	30.0	78.1	14.9	13.3	6.5
I-FGSM	31.4	25.3	23.1	99.3	8.7	8.5	5.4
MI-FGSM	57.6	51.9	49.8	99.3	23.9	22.1	12.6
NI-FGSM	65.5	58.0	57.5	99.4	24.3	21.5	11.3
PI-FGSM (Ours)	72.8	66.8	63.7	99.3	28.3	25.3	14.0
EMI-FGSM (Ours)	82.3	76.7	76.2	100.0	35.2	30.8	19.0

(c) Attack success rates (%) for the adversarial examples crafted on **Res-101**.

Table 6: **Attack success rates (%) of various adversarial attacks against the seven baseline models under single-model setting.** The adversarial examples are crafted on **Inc-v4**, **IncRes-v2** or **Res-101** using various adversarial attack methods. * indicates the white-box model being attacked.

Attack	Inc-v3	Inc-v4*	IncRes-v2	Res-101	Inc-v3 _{ens3}	Inc-v3 _{ens4}	IncRes-v2 _{ens}
DIM	74.1	98.5	66.3	58.0	22.3	21.0	11.6
EMI-DIM (Ours)	89.4	99.1	83.6	75.2	33.5	30.9	16.7
TIM	58.0	99.5	47.2	42.8	25.9	24.0	16.9
EMI-TIM (Ours)	89.0	99.8	81.2	72.3	52.1	48.3	35.2
SIM	80.6	99.5	73.6	68.8	47.9	44.9	29.2
EMI-SIM (Ours)	96.4	99.9	93.7	89.0	59.7	56.1	36.9
DTS	84.7	98.0	80.5	76.3	67.9	66.9	54.3
EMI-DTS (Ours)	95.7	99.4	94.5	90.7	81.4	77.5	68.8

(a) Attack success rates (%) for the adversarial examples crafted on **Inc-v4**.

Attack	Inc-v3	Inc-v4	IncRes-v2*	Res-101	Inc-v3 _{ens3}	Inc-v3 _{ens4}	IncRes-v2 _{ens}
DIM	68.1	65.1	93.7	58.3	30.2	23.4	17.3
EMI-DIM (Ours)	88.8	85.1	98.5	78.3	42.4	35.5	26.4
TIM	62.1	55.8	97.2	49.9	31.0	28.3	21.5
EMI-TIM (Ours)	90.6	85.0	99.4	80.1	61.5	52.2	48.2
SIM	84.6	79.5	98.9	76.1	55.9	49.0	41.7
EMI-SIM (Ours)	97.5	95.1	99.9	90.9	69.0	60.1	51.6
DTS	87.1	84.3	96.6	81.4	76.4	73.3	69.4
EMI-DTS (Ours)	97.8	95.4	99.9	93.6	88.2	83.5	81.9

(b) Attack success rates (%) for the adversarial examples crafted on **IncRes-v2**.

Attack	Inc-v3	Inc-v4	IncRes-v2	Res-101*	Inc-v3 _{ens3}	Inc-v3 _{ens4}	IncRes-v2 _{ens}
DIM	73.6	68.5	69.5	97.6	36.2	31.9	20.6
EMI-DIM (Ours)	88.7	84.3	84.1	99.7	46.4	40.7	26.3
TIM	59.4	54.0	52.3	99.2	35.6	31.8	22.8
EMI-TIM (Ours)	86.0	79.1	79.8	100.0	56.4	50.3	41.7
SIM	74.4	69.8	68.3	99.7	43.1	39.4	26.0
EMI-SIM (Ours)	92.0	88.7	88.4	100.0	57.6	50.4	35.7
DTS	84.0	80.0	81.9	98.9	73.3	70.9	59.3
EMI-DTS (Ours)	93.7	90.9	92.3	99.6	83.9	80.9	71.7

(c) Attack success rates (%) for the adversarial examples crafted on **Res-101**.

Table 7: **Attack success rates (%) of various adversarial attacks against the seven baseline models under single-model setting.** The adversarial examples are crafted on **Inc-v4**, **IncRes-v2** or **Res-101** using various adversarial attack methods. * indicates the white-box model being attacked.